# A Novel Voltage Collapse Path Analysis of Primary System Equivalent Model for Smart Grid

JIE XU, (Member, IEEE), AND WENGEN GAO
Key Laboratory of Advanced Perception and Intelligent Control of High-End Equipment, Ministry of Education, Anhui Polytechnic University, Wuhu 241000, China

Corresponding author: Wengen Gao (ahpuchina@ahpu.edu.cn)

**ABSTRACT** This paper proposes a novel equivalence model of the smart grid. The smart grid can be equivalent to a three-layer model, namely power supply, power distribution, and power layer. For equivalent model, the system voltage collapses path are analyzed, the characteristics of the N structure complex smart grid model are derived. The weighted graph model of the brittle relationship of complex smart grid systems is analyzed. The model has the characteristics of logical clarity, hierarchical representation, qualitative analysis. By finding the crash path through different equivalent modes, the crash state path between subsystems can be analyzed. The voltage collapse of one node in the operation of the smart grid system will be transmitted to the entire system through a chain reaction, which will cause the entire system to collapse. The maximum voltage collapse path for different equivalent modes is used to analyze the most likely collapse path. The method of predicting and controlling the brittle voltage collapse path of the smart grid can effectively optimize the performance of the entire system, which has important guiding significance for the design and control of the smart grid.

**INDEX TERMS** Equivalent model, smart grid, voltage collapse path.

## I. INTRODUCTION

The quantitative analysis of voltage collapse in complex power systems has been a hot topic of research. Voltage collapse detection concepts of voltage support surface and local balancing equation are also proposed [1]. The model for analyzing the complex system's brittleness has been considered [2]. There are few studies on brittleness in smart grid environments, brittleness is an inherent property of the system in complex system brittle structural model [3], [4]. A distributed linearity for calculating the voltage collapse sensitivity index online has been successfully applied in ship power system [5].

European countries are in a leading position in the research of system fragility, and have applied the research results of fragility to various fields such as national defense security, transportation, industry, etc [6]. And some scholars use new method processes the relevant data of the power system, and has completed the research on the vulnerability of power

The associate editor coordinating the review of this manuscript and approving it for publication was S. Srivastava.

systems such as substations [7]. At the same time, it has been researched that when a certain substation or other key equipment in the system fails, it will lead to the research including the breakdown of the entire system.

In the 21st century, with the development of distributed power generation systems and smart grids, mankind has carried out a new power grid era [8]–[11], which obtain a series of research on smart grids, and also put forward a new perspective on smart grid security, including heavy-load attacks. The impact of the interference on the smart grid [12]–[14], the access of new energy in the smart grid, the research on the stability of smart grid have begun to be a hot spot, and the problem of voltage fluctuations including the voltage collapse limit state has been studied in depth [1], [15], [16], which is also the commonality of system fragility. The stability, safety, and controllability of smart grids have become the main research directions in the development of smart grids, and new requirements have been put forward for the research of smart grids.

Recent years have brought development, good foundations for the research of brittleness theory of smart grid system has

received some more research results [17], [18]–[22], which will have important guiding significance for the research of smart grid system. The introduction of new methods provides research directions for the research on the voltage collapse path, some papers propose relaxed decoupled direct calculation method to find voltage collapse points [23], [24]. The hardware and local algorithm are used to study the voltage collapse path [25]–[27].

The complex smart grid is the research object, with power supply, storage capacity, new energy access, load, etc. The study of system collapse behavior is a novel thinking direction for smart grid research and has practical guiding significance. There are many reasons for the failure of the complex smart grid, especially the voltage fluctuation, and some will have serious consequences such as the collapse of the entire system. The fragility in the system is different from the general system failure. Compared with the traditional particle swarm optimized(PSO) optimization problem [34], [35], it is easy to fall into the local optimum. In this paper, the logistic PSO velocity update formula with random white noise is added to ensure the continuous update of velocity when the particle is about to fall into the local optimum.

This paper discusses the characteristics of the particle swarm optimization algorithm and uses it to solve the problem of the largest collapse path of the complex smart grid system. The simulation of the smart grid system provides a basis for predicting and controlling the brittle behavior of the system under extreme voltage collapse. This paper analyzes the limit state of the system with different working modes, which provides methods of limit state analysis.

## II. PRIMARY ELECTRICAL SYSTEM MODELING OF MAIN TOPOLOGY

### A. TWO THREE-LAYER EQUIVALENT MODELS OF THE SYSTEM

The paper analyzes the voltage limit state through the AGENT diagram. Equivalent model of primary system is based on 35kV smart grid. The system layout is shown in Figure1. The design of the primary system based on 35kV smart grid is mainly based on 380V adjustable transformer to 800V analog 35kV core control system, using main line power supply, wind power generation, solar power supply, real-time switching equipment, intelligent and safe power supply. The system consists of various modules, consisting of busbars, transformers, bidirectional converters, filters, iron-lithium batteries, capacitors, hydropower and thermal power generation, photovoltaics, solar power generation and other modules. Main parameters (1) Doubly-fedfans: for simulation 35kV system, so the wind turbine generator-dual-fed fan of small household is selected, its rated capacity is 5kW to meet the requirements. (2) iron-lithium battery: the model of iron-lithium battery is 20kW, which belongs to small household energy storage equipment. The output power of the supporting inverter is 6kVA. (3) Super capacitor: the selection of super capacitor, its rated capacity output power is $0 \sim 20$kW.
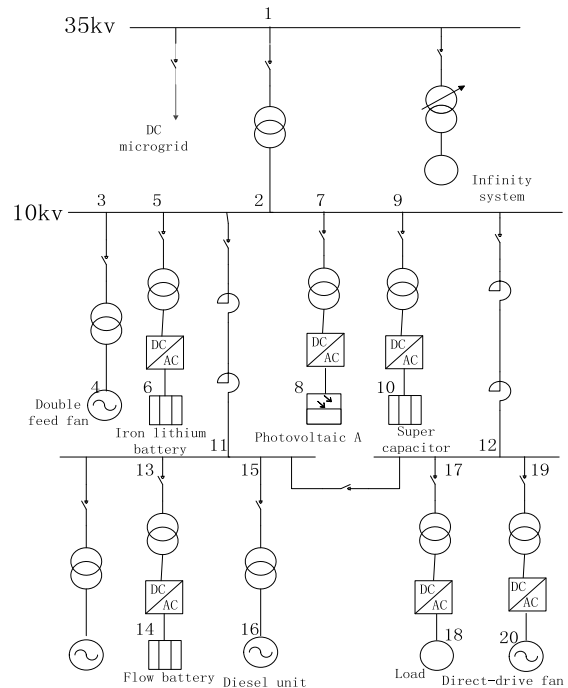


**FIGURE 1.** Energy storage power model of wind and solar energy.

(4) Photovoltaic power generation: the selected photovoltaic is also a small household photovoltaic power generation rated capacity is 8kW (for general household small photovoltaic 2-5kW that meets the requirements; The inverter operating frequency is 90%.) (5) Flow battery. (6) Diesel drive unit. (7) Direct drive motor.

In order to study the brittleness of complex smart grid systems, the equivalent models are analyzed and discussed separately to provide a basis for further study of system brittleness [5], [28]–[31]. In this paper, the smart grid system is divided into different levels according to several functional modules of power supply, power distribution and power consumption, and then further subdivided into subsystems.

Smart grids mainly operate in two modes: on-grid and off-grid. One is to connect the smart grid to the main grid, and the other is to cut off the main grid. The research models in this paper are divided into on-grid model A and off-grid model B.

After analyzing the structure, a three-layer equivalent model can be established: power supply layer, distribution layer, and electricity consumption layer. The three-layer equivalent model is applicable to any smart grid structure. Corresponding to the two modes of grid-connected operation and off-grid operation of smart grid, the power layer of model A and model B are also different. The power supply layer is provided by wind power, photovoltaic power generation and the main power grid, which is called model A in Figure2. When the smart grid is in the off-grid state, the power layer of model A will leave the main grid to form model B. The iron-lithium battery and supercapacitor in model A can store and discharge due to their physical characteristics, and they are also incorporated into the power supply layer. As model B,
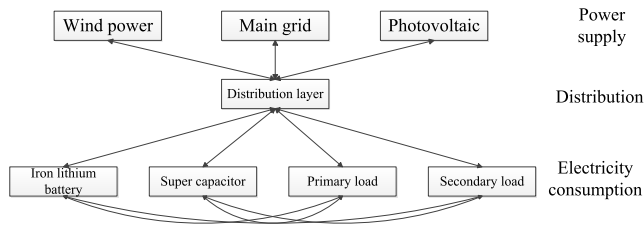
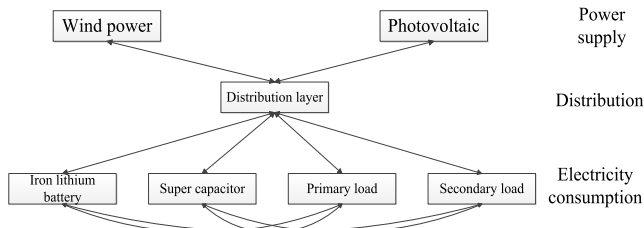**FIGURE 2.** Power model of wind and solar energy in grid-connected mode.



**FIGURE 3.** Power model of wind and solar energy in off-grid mode.

wind energy storage power supply model for analysis is shown in Figure3.

The smart grid system is divided into several functional modules, such as power supply, power distribution and electricity consumption. On this basis, it is further subdivided into subsystems, and the relationship between subsystems is considered. This is the equivalent model of smart grid.

## B. ANALYSIS OF EQUIVALENT MODEL AGENT WEIGHTING GRAPH IN SYSTEM

With the development of different nature power sources in the smart grid system as the system power source, the system may cause the voltage collapse of the system under abnormal operation, the number of crash subsystems recursively increases, the expansion will eventually lead to the collapse of the entire complex system with serious consequences. The edge of the graph is used to describe the brittle connection between subsystems, and the weight of the edge is used to describe the degree of brittle connection between subsystems. Through effective control algorithm, the possible collapse path of smart grid when brittleness occurs is analyzed, which is the voltage collapse path.

For the system in a state of possible collapse, it is necessary to discuss the state before the crash, thus giving the concept of brittleness of the smart grid system [5]. There are many reasons why the smart grid system cannot operate normally, but some do not cause the entire system to crash. The system crash is a state under extreme operation and the final system state under various interference conditions.

In order to study the brittleness of the system more conveniently, the brittleness diagram of the smart grid system is represented as an adaptive graph model [17], [32], [33]. Each subsystem of the system is an adaptive agent, and the brittleness of the smart grid system is established by using the brittle relationship between subsystems as the topological structure. This paper applies the adaptive graph model
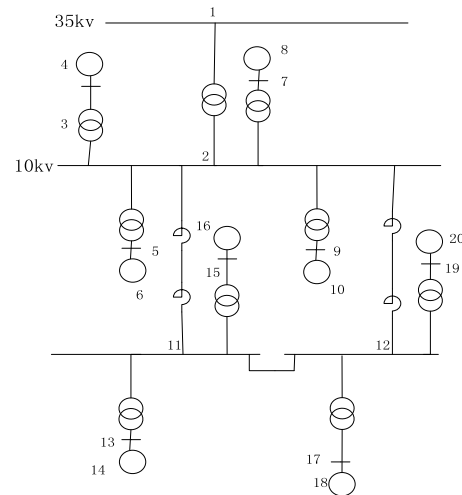


**FIGURE 4.** Agent weighted graph of energy storage power model with double feed fan and iron lithium battery.
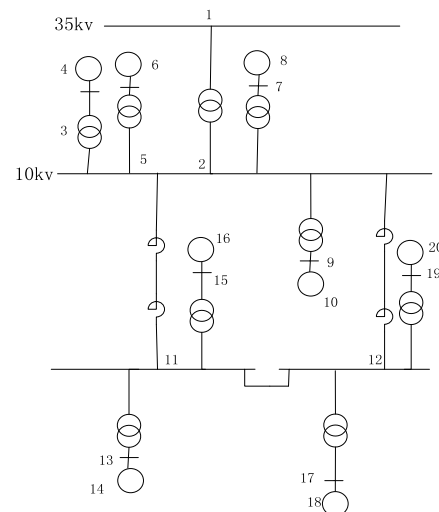


**FIGURE 5.** Model agent weighting diagram double feed fan and iron lithium battery.

to analyze the dynamic characteristics of brittle behavior between subsystems in the smart grid system.

For the brittleness study of smart grid systems, this paper describes the system through the weight graph, and only consider the brittle relationship of the system: each subsystem is a node, and the degree of brittleness between the subsystems is the edge, brittleness agent weighting graph model for smart grid systems.

In mode 1, the power supply layer is composed of a fan, a photovoltaic, a diesel unit, a direct-drive fan, and a lithium-lithium battery, as shown in Figure4, this is a smart grid that is independent of the main grid and is operating in an off-grid mode.

In addition to these two modes, the brittle relationship between systems in the non-off-grid state of the smart grid continues to establish five topologies to discuss the topology of the small modules in the power generation unit and the
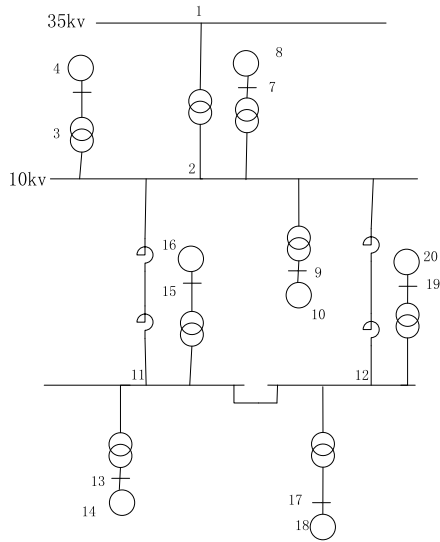
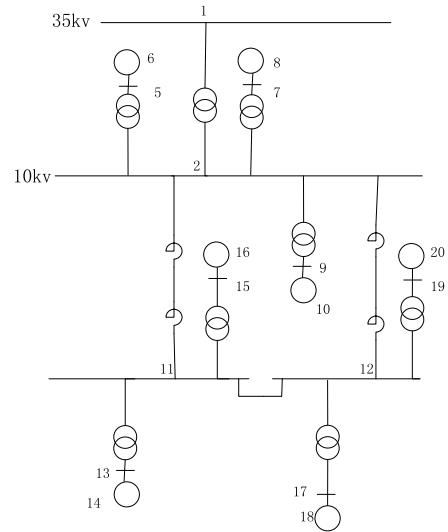**FIGURE 6.** Model agent weighting diagram with double feed fan.



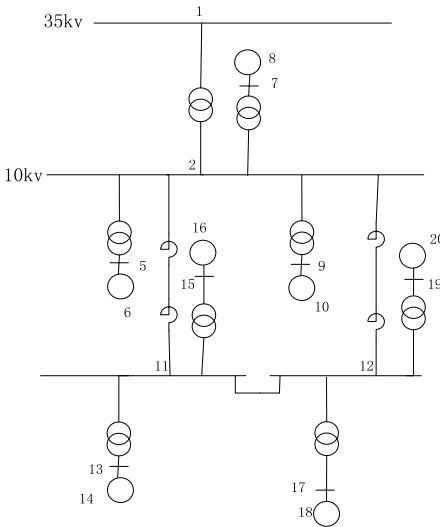**FIGURE 8.** Model agent weighting diagram with iron lithium battery.



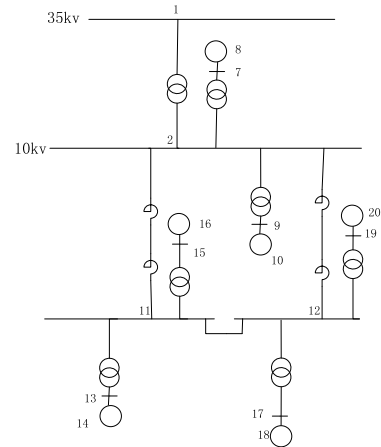**FIGURE 7.** Model agent weighting diagram with iron lithium battery.



**FIGURE 9.** Model agent weighting diagram without double feed fan and iron lithium battery.

chargeable and discharge unit. The overall topology of the entire large system can be expanded.

In mode 2, the power supply layer is considered to be a fan, photovoltaic, iron-lithium battery, diesel unit, direct-drive fan, and the rest are loads in Figure5.

In mode 3, the power supply layer is composed of a fan, a photovoltaic, a diesel unit, a direct-drive fan, and the rest is a load, but the load is removed from the iron-lithium battery in Figure6.

In mode 4, Figure. 7 shows that the power layer photovoltaic, diesel units, direct drive fans, the rest for the load.

In mode 5, the power supply layer is composed of photovoltaic, diesel unit, direct drive fan and iron-lithium battery, and the rest is load, as shown in Figure8.

In mode 6, the power supply layer consists of photovoltaic, diesel, direct-drive fans, and the rest is the load, but the load is removed from the iron-lithium battery in Figure9.

## III. MATHEMATICAL MODEL ANALYSIS

### A. PARTICLE SWARM OPTIMIZATION

The particle swarm optimization algorithm is an evolutionary computation technique, which is proposed by Eberhart and Kennedy, from the behavioral study of predation of birds.

When c is used to solve the maximum collapse path of smart grid, it is assumed that n particles are randomly distributed on each node of the fragility weighting graph model of the micro grid system [5], [34]–[36], and the initial population of particles is randomly generated. Each particle has a random initial speed. The following equations update particle velocity and particle position:

$$V_{id}^{k+1} = \omega V_{id}^{k} + c_1 r_1 \left( P_{id}^{k} - X_{id}^{k} \right) + c_2 r_2 \left( P_{gd}^{k} - X_{id}^{k} \right) \quad (1)$$

$$X_{id}^{k+1} = X_{id}^{k} + V_{id}^{k+1} \quad (2)$$

$$\omega = \frac{\omega_{\max} - \omega_{\min}}{MaxIt} iter \tag{3}$$

where $\omega$ is the inertia weight, $d = 1, 2, \ldots, D$; $i = 1, 2, \ldots, n$; $X_{id}$, $V_{id}$ represents the current position of the particle and the particle velocity; $c_1$ and $c_2$ are non-negative constants, called acceleration factors, Here $c_1 = 0.5$, $c_2 = 0.7$; $r_1$ and $r_2$ are random numbers distributed in the interval [0,1]. Pid and Pgd represent the current best position of the particle and the current best position in the population. iter $= 1, 2, \ldots,$ MaxIt. MaxIt represents the maximum number of iterations, $\omega_{\max}$, $\omega_{\min}$ represents the maximum inertia weight and the minimum inertia weight.

### B. RESEARCH ON MATRIX IN ALGORITHM

For n*n-type matrices, there are generally such matrix representations.

$$Q = \begin{bmatrix} q_{11} & q_{12} & \cdots & q_{1n} \\ q_{21} & q_{22} & \cdots & q_{2n} \\ \vdots & \vdots & & \vdots \\ q_{n1} & q_{n2} & \cdots & q_{nn} \end{bmatrix}_{n \times n} = (q_{ij})_{n \times n} \tag{4}$$

The n*n-type matrix represents an n-dimensional topology. The specific value of n depends on the number of connected topologies. The Q represents the n*n-type matrix, and the $q_{ij}$ represents the value of the i-th row and the j-th column in the matrix. Due to the particularity of the matrix used by the algorithm, the matrix is a symmetric matrix, it is clear that

$$\begin{aligned} q_{ij} &= q_{ji} \\ q_{ii} &= 1 \end{aligned} \tag{5}$$

The above matrix will be divided into blocks, and the block matrix is obtained as follows.

$$\begin{bmatrix} A & C \\ B & D \end{bmatrix} \tag{6}$$

where A, B, C, and D represent the respective block matrices, among them,

$$A = \begin{bmatrix} a_{11} & \cdots & a_{1m} \\ \vdots & \ddots & \vdots \\ a_{m1} & \cdots & a_{mm} \end{bmatrix}_{m \times m} \tag{7}$$

In matrix A, $a_{ij}$ is used to represent the matrix values of the i-th row and the j-th column.

Matrix A is a symmetric matrix, in the matrix A:

$$\begin{aligned} a_{ii} &= 1 \\ a_{ij} &= a_{ji} \end{aligned} \tag{8}$$

Each matrix A is fixed and has the following matrix. Rank of matrix A:

$$\text{Rank (A)} = m \tag{9}$$

$$B = \begin{bmatrix} b_{11} & \cdots & b_{1i} & b_{1(i+1)} & \cdots & b_{1(n-m)} \\ \cdots & \cdots & \cdots & \cdots & \cdots & \cdots \\ b_{m1} & \cdots & b_{mi} & b_{m(i+1)} & \cdots & b_{m(n-m)} \end{bmatrix}_{m \times (n-m)} \tag{10}$$

In matrix B, $b_{ij}$ represents the value of the i-th row, the j-th column, and has a total of m rows, (n-m) columns.

According to the three-layer topology model, it is assumed that the number of topologies directly related between the first layer and the second layer is m, and there is no direct relationship between the second layers, and the number of indirect links between the third layers is a, the number of topologies without indirect links is b. This paper introduces a concept, for the three-layer topology, we think that the relationship between the first and second layers is a simple direct relationship, and the relationship between the second layers is more complicated. We classify as follows: Assume that the number of sub-topologies are not associated is a, and

$$b_{in} = \begin{cases} b_{i1} - 0.2(n-1) & n < 5 - j \\ 0 & n \geq 5 - j \end{cases} \quad 1 \leq i \leq m$$

$$b_{1j} = \begin{cases} 0 & j = 1 \\ 1.3 - 0.2j & 2 \leq j \leq 6 \\ 0 & j \geq 7 \end{cases} \tag{11}$$

Rank of matrix B:

$$\text{Rank (B)} = \begin{cases} m - 1 & m \leq 6 \\ 5 & m \geq 7 \end{cases} \tag{12}$$

the number of indirect associated sub-topologies is b. At the same time, the value of a affects the value of the B and C matrices. In theory, the maximum value of a is 5, and for the associated sub-topology greater than 5, it can be considered as uncorrelated, with a value of 0. In the maximum crash path algorithm, points with a value of 0 cannot be brought into the operation matrix [5]. Therefore, all points with a value of 0 will be replaced by 0.1 to represent irrelevant points in the topology.

In the algorithm of the maximum crash path, we assume that the value of the point with a value of 0 is 0.1 to replace the irrelevance between points: rank(B) = m − 1

Regardless of its substitute value, only the basic matrix structure is discussed.

The C matrix is discussed below, wherein the C matrix is similar to the B matrix and is a symmetric matrix of the B matrix, which will not be described here.

$$\begin{bmatrix} c_{11} & \vdots & c_{(n-m)m} \\ \vdots & \vdots & \vdots \\ \vdots & \vdots & \vdots \\ \vdots & \vdots & \vdots \\ \vdots & \vdots & \vdots \\ \vdots & \vdots & \vdots \\ c_{(n-m)1} & \vdots & c_{(n-m)m} \end{bmatrix}_{(n-m) \times m} \tag{13}$$

$$c_{ni} = \begin{cases} c_{1\,i} - 0.2(n-1) & n < 5 - j \\ 0 & n \geq 5 - j \end{cases} \quad 1 \leq i \leq m$$

$$c_{j1} = \begin{cases} 0 & j = 1 \\ 1.3 - 0.2j & 2 \le j \le 6 \\ 0 & j \ge 7 \end{cases} \tag{14}$$

where $c_{ij}$ represents the value of the i-th row and the j-th column in the matrix C, and has a total of (n-m) rows and m columns. Matrix D is the most complex, and it is again partitioned here. Four block matrices of D1, D2, D3, and D4 are obtained, eq (15), as shown at the bottom of the page.

As with the matrix above, it has been partitioned and constrained by several equations.

$$\begin{cases} d1_{ii} = 1 \\ d1_{ij} = d1_{ji} = 0 \\ d2_{ii} = \begin{cases} 0.7 - 0.2n & 1 \le n \le 3 \\ 0 & n \ge 4 \end{cases} \\ d2_{ij} = d2_{ji} = 0 \\ d3_{ii} = \begin{cases} 0.7 - 0.2n & 1 \le n \le 3 \\ 0 & n \ge 4 \end{cases} \\ d3_{ij} = d3_{ji} = 0 \\ d4_{ii} = 1 \\ d4_{ij} = d4_{ji} = 0 \end{cases} \tag{16}$$

where $c_{ij}$ represents the value of the i-th row and the j-th column in the matrix C, and has a total of (n-m) rows and m columns.

It is known that the D matrix is composed of a unity symmetric matrix and a symmetric matrix whose oblique diagonals are arithmetic progressions, wherein the first term of the arithmetic progression is 0.7 and the common ratio is −0.2. We assume that each value of the diagonal is D21, D22 ... D2n, and the values after n > 3 are held at zero, which constitutes the 0 matrix of the lower right corner. At the same time, the value of b affects the change in the value of the D matrix, and the maximum value of b should be 4. The D matrix has a special feature. The order of the matrix is increased by an even pair, so the D matrix is always an even order matrix. It can be seen from the above equations that the four matrices are all symmetric matrices, at the same time, the value of 0 is all replaced by 0.1. Using MAT-LAB to analyze the above matrix, we can conclude that the

orthogonal space of the above matrix is the identity matrix. That is, the specific value of l is based on the order of the matrix.

$$\begin{bmatrix} 1 & \cdots & 1 \\ \vdots & \ddots & \vdots \\ 1 & \cdots & 1 \end{bmatrix}_{l \times l} \tag{17}$$

Simultaneously solving the traces of each matrix can be obtained,

$$\begin{cases} -0.1\,n^2 + 0.8\,n & D2, D3 \\ 1 & D1, D4 \end{cases} \tag{18}$$

From the above two Equations (17) and (18), it can be concluded that it is consistent with the derivation process. This is only for the discussion of simple topology, but the idea can be derived into the n*n matrix to get the general structure of the matrix Q.

## IV. SIMULATION MODEL AND RESULT ANALYSIS

The above topology graphs are simulated and analyzed, and the main simulation parameters are as follows:

(1) *P:* It is the total number of particles in the population, set to a value between 10 and 40, based on the complexity of the smart grid, the total number of particles is 100.

(2) *Dim:* The motion interval between particles is determined by optimizing the problem. For different topologies of the smart grid, the motion space of the particle has three dimensions, which are 20 dimensional, 18 dimensional, 16 dimensional. Each dimension can be set in its different interval.

(3) *d:* It is the specific situation of the optimization problem to make a decision.

(4) *ω:* Inertia weight, which keeps the particles inert, and expands the search space and opens up new areas. Considering the update of the particle optimization speed, the maximum inertia weight and the minimum inertia weight are set, and the inertia weight is updated by the loop iteration by the maximum iteration number of the particle according to Equation (3).

(5) *V*$_{max}$*:* The maximum speed determines the range of maximum movement of the particle, and is generally set to the

$$D = \begin{bmatrix} d1_{11} & d1_{12} & d1_{13} & d3_{11} & \cdots & \cdots & \cdots & \cdots & d3_{1(n-m-3)} \\ d1_{21} & d1_{22} & d1_{23} & \cdots & \cdots & \cdots & \cdots & \cdots & \cdots \\ d1_{31} & d1_{32} & d1_{33} & d3_{31} & \cdots & \cdots & \cdots & \cdots & d3_{3(n-m-3)} \\ d2_{11} & d2_{12} & d2_{13} & d4_{11} & \cdots & \cdots & \cdots & \cdots & d4_{1(n-m-3)} \\ \vdots & \vdots & \vdots & \cdots & \cdots & \cdots & \cdots & \cdots & \cdots \\ \vdots & \vdots & \vdots & \cdots & \cdots & \cdots & \cdots & \cdots & \cdots \\ \vdots & \vdots & \vdots & \cdots & \cdots & \cdots & \cdots & \cdots & \cdots \\ \vdots & \vdots & \vdots & \cdots & \cdots & \cdots & \cdots & \cdots & \cdots \\ d2_{(n-m-3)1} & d2_{(n-m-3)2} & d2_{(n-m-3)3} & d4_{(n-m-3)1} & \cdots & \cdots & \cdots & \cdots & d4_{(n-m-3)(n-m-3)} \end{bmatrix}_{(n-m-3) \times (n-m-3)} \tag{15}$$

width of the particle's active range. Where $V_{max}$ is too high, the particles may cross better solutions and lose their ability. If $V_{max}$ is small, the particles cannot be explored outside the local interval, resulting in local extremum.

(6) *Learning Factor:* Keeping particles in motion inertia, so that they have the ability to expand the search space and explore new areas, this performance is the main feature of the particle algorithm. The main parameters are c1 and c2, which represent the weight of each particle to the best position and the statistical acceleration of the best position. This is the usual method of setting parameters.

(7) *Maximum Number of Iterations:* The algorithm terminates the condition, and the value is determined by the specific problem. Select 500 here as the maximum number of iterations.

(8) $\chi$ is called the compression factor, which acts on w, and is used to control its convergence speed. This factor has no significant impact on the algorithm, the parameter setting is clear, we must consider the quality and calculation cost of the case 6 in two aspects.

The following is a discussion of the random crash path, the optimal collapse path, the fitness curve and the particle velocity curve under different supply and discharge devices. Figure. 10 to Figure. 13 are simulation diagrams under model 1.

Figure10 is a random crash path, from which it can be seen that the occurrence of the crash is random, but the collapse of one point will affect other stores and the chain reaction will cause the entire system to collapse, which explains the impact of random crash on the whole. We study one of the random examples, but it is representative.
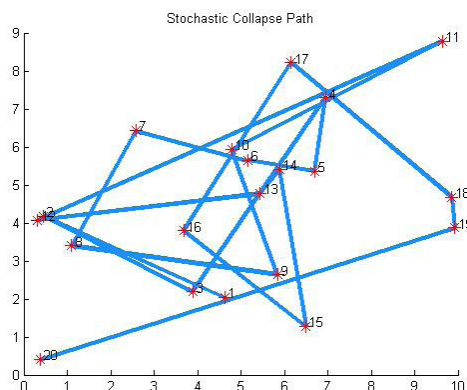


**FIGURE 10.** Chart of stochastic collapse path with model 1.

As shown in Figure11 is the optimal crash path. Through the particle swarm optimization algorithm, the crash path is continuously iterated and optimized. Finally, a road with the largest brittleness of the crash path R in the specified range is found. In this case, the system crash loss. Minimize, minimize the damage caused by the crash.

Figure. 12 is the fitness change curve. As the number of iterations increases, the particle fitness becomes larger, that
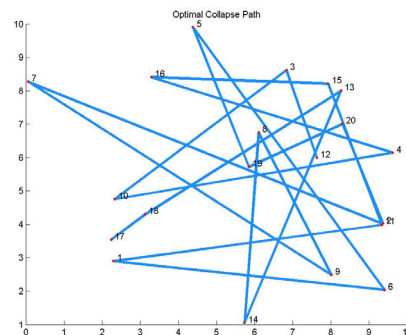


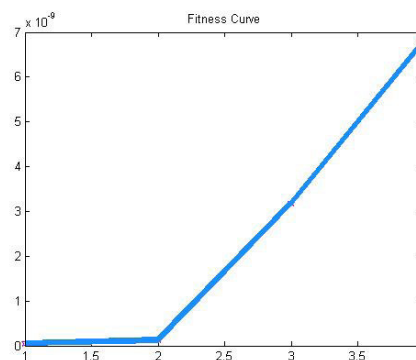**FIGURE 11.** Chart of optimal collapse path with model 1.



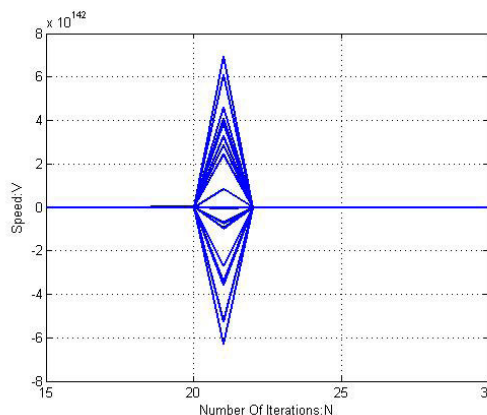**FIGURE 12.** Chart of fitness curve with model 1.



**FIGURE 13.** Chart of velocity curve with model 1.

is, the brittleness weight of the crash path R becomes larger, which is the same as the expected result: the final fitness tends to a certain value.

It can be seen that the velocity of each iterative particle is recorded in the process of particle iterative optimization. In the process of updating the speed shown in Figure13, the speed will have an extreme value, and finally it will go to 0.
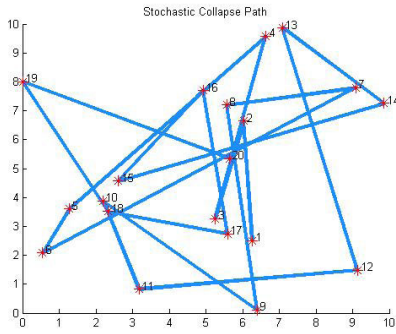
$$\lim_{x \to \infty} v_n = 0 \qquad (19)$$

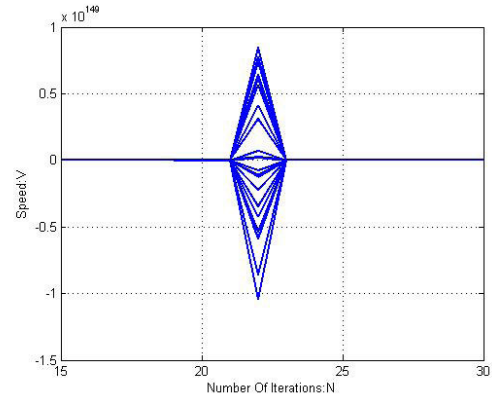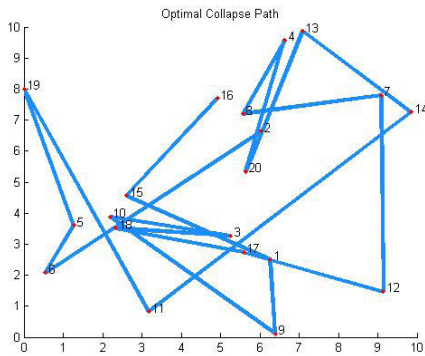**FIGURE 14.** Chart of stochastic collapse path with model 2.



**FIGURE 15.** Chart of optimal collapse path with model 2.



**FIGURE 16.** Chart of fitness curve with model 2.



**FIGURE 17.** Chart of velocity curve with model 2.



**FIGURE 18.** Chart of stochastic collapse path with model 3.



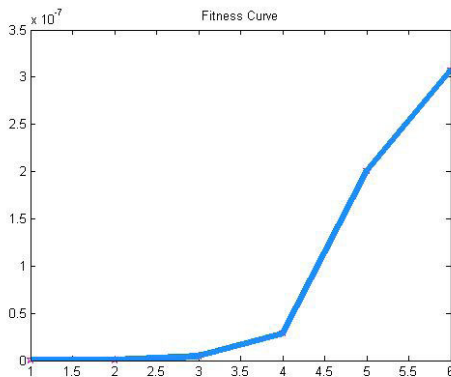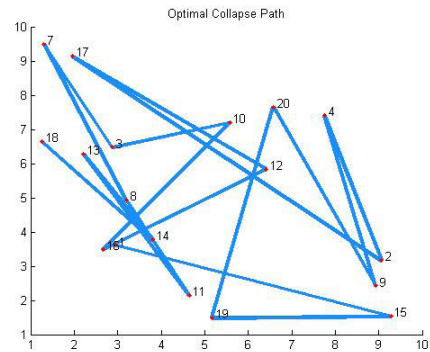**FIGURE 19.** Chart of optimal collapse path with model 3.

where Vn represents the velocity of motion of the particle group.

1) The optimal path is:

12-3-10-4-16-15-11-1-6-5-19-20-2-7-9-8-14-13-18-17

Figure. 14 to Figure. 17 are simulation diagrams under model 2. The discharge and discharge device of model 2 has undergone a slight change with respect to the model 1. It can be seen that the optimal collapse path of the system changes with the change of water supply and discharge device, but the whole fitness trend changes little, and the particle velocity with the change tends to zero.

2) The optimal path is:

2-6-5-19-11-14-13-20-4-8-7-12-17-18-3-10-9-1-15-16

As shown in Figure18 to Figure21, the simulation diagram under the model 3 shows that the optimal crash path change of the system is obvious due to the removal of the power supply of the iron-lithium battery. Compared with the simulation diagrams under model 1 and model 2, the overall fitness of the system changes little, but the overall fitness change rate is very fast, the slope of the curve changes greatly, and particles will approach zero at a faster rate.

3) The optimal path is:
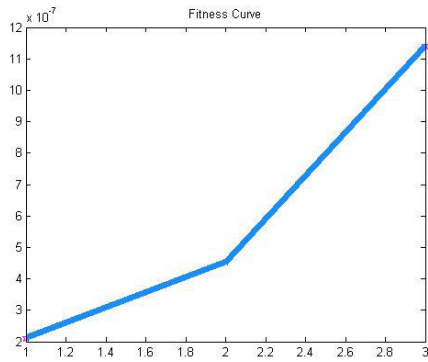
1-15-19-20-9-4-2-17-12-16-10-3-7-8-11-13-14-18

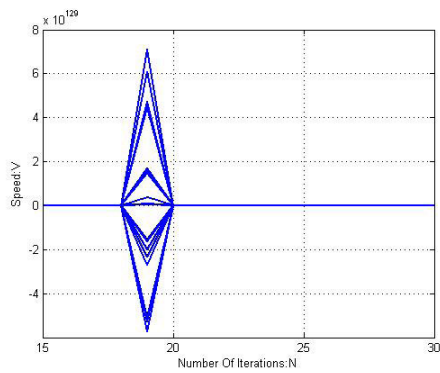**FIGURE 20.** Chart of fitness curve with model 3.
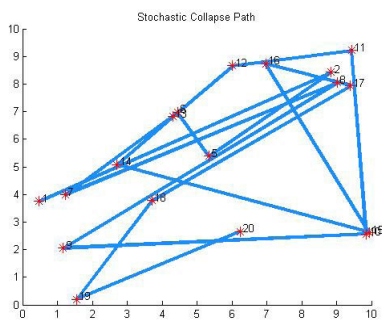


**FIGURE 21.** Chart of velocity curve with model 3.



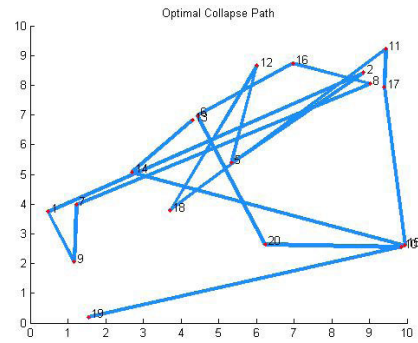**FIGURE 22.** Chart of stochastic collapse path with model 4.



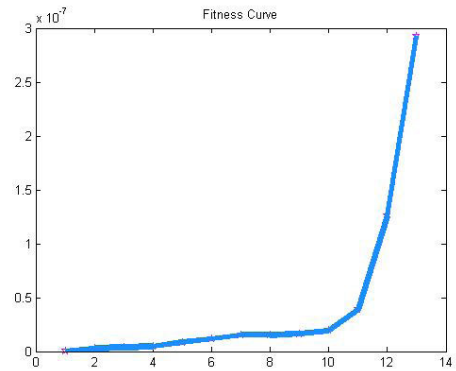**FIGURE 23.** Chart of optimal collapse path with model 4.



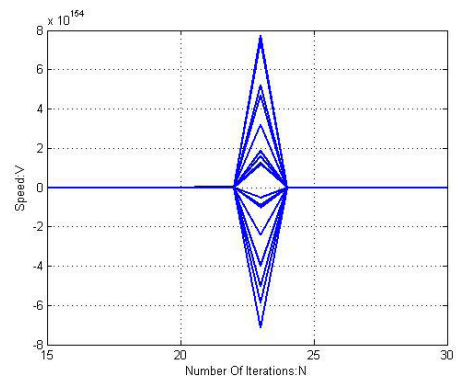**FIGURE 24.** Chart of fitness curve with model 4.



**FIGURE 25.** Chart of velocity curve with model 4.

Figure22 to Figure25 are simulation diagrams under the model 4. At this time, the discharge device changes greatly, but the overall trend of the simulation chart changes little, and the velocity of the particles still tends to zero, but the rate of change is slightly different.

4) The optimal path is:

19-10-20-6-16-8-7-9-1-2-5-12-18-11-17-15-14-13

Figure26 to Figure29 are simulation diagrams under model 5. Compared with model 4, the change of fitness is more obvious when the iron-lithium battery is used as the power supply device. When the iron-lithium battery is used as the load, as shown in Figure28, The degree of change in the beginning of the curve is relatively stable, and then suddenly

changes greatly. However, when the iron-lithium battery is used as the power supply device, a large slope change occurs in a short time, indicating that changing the position of the same device has a great influence on the crash path. At the same time, the velocity of the particles that changes with it still tends to zero.

5) The optimal path is:

14-13-5-6-19-20-2-7-8-1-11-15-10-9-12-17-18-16

Figure30 to Figure33 are simulation diagrams under model 6. After removing the iron-lithium battery and the doubly-fed fan, the overall change trend of the system is not large. At this time, the crash path is simpler, and the
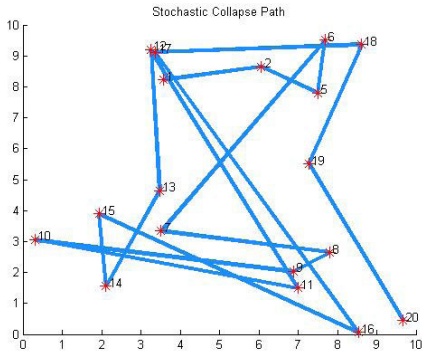
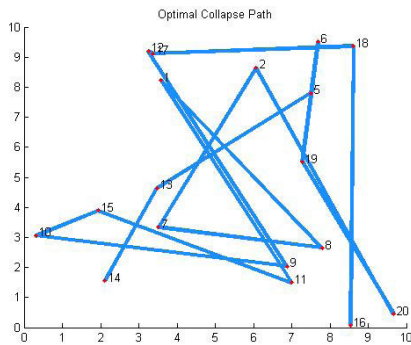**FIGURE 26.** Chart of stochastic collapse path with model 5.



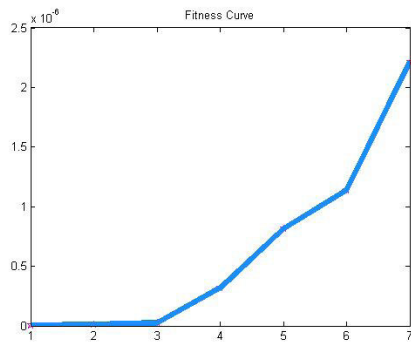**FIGURE 27.** Chart of optimal collapse path with model 5.



**FIGURE 28.** Chart of fitness curve with model 5.



**FIGURE 29.** Chart of velocity curve with model 5.



**FIGURE 30.** Chart of stochastic collapse path with model 6.
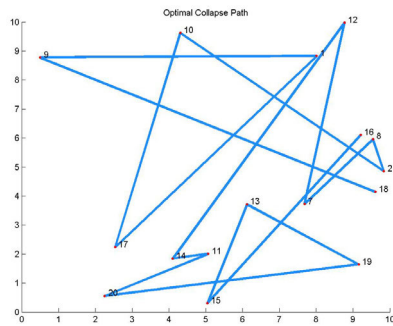


**FIGURE 31.** Chart of optimal collapse path with model 6.
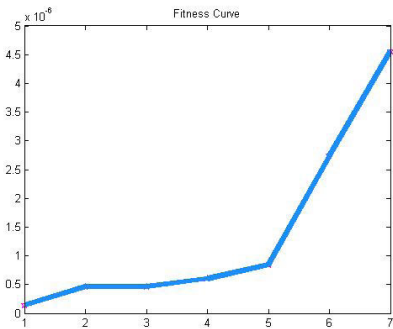


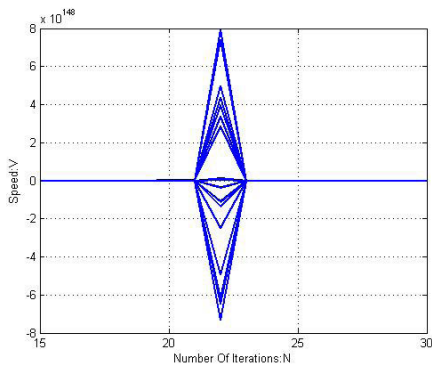**FIGURE 32.** Chart of fitness curve with model 6.



**FIGURE 33.** Chart of velocity curve with model 6.

overall fitness of the system changes little. However, the rate of change in fitness at the beginning is only a little larger. The particle velocity still tends to 0.

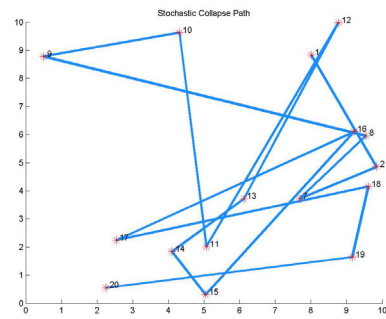6) The optimal path is:
18-9-1-17-10-2-8-7-12-14-11-20-19-13-15-16
It can be seen from the above structural topologies that the overall fitness curve changes according to the general trend, changes from a certain point, and after a certain degree,
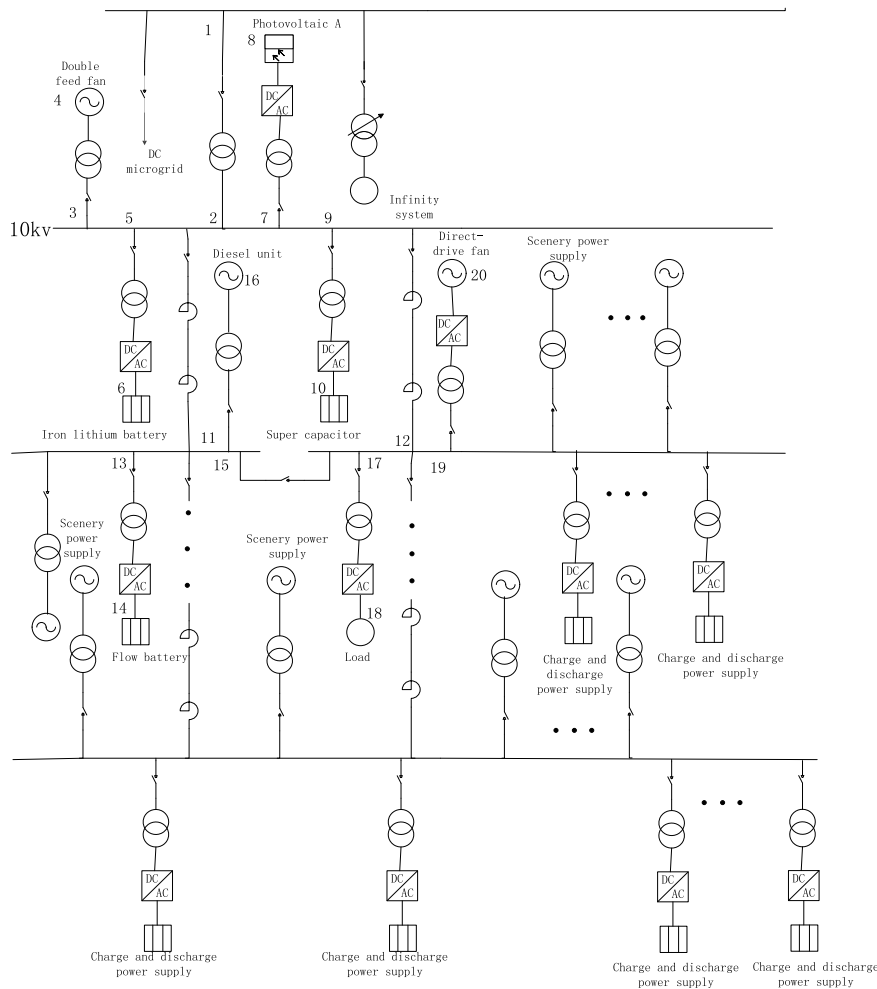
**FIGURE 34.** Topology diagram of smart grid.

the slope will change a lot and the degree of adaptation will be greatly improved. A lot of enhancements, combined with the crash path that has occurred, it is seen that the occurrence of the crash point is random and then spread to each endpoint, which can cause the entire system to crash. The reason why we study the above system is that it is a small topology, and thus the structure can derive the overall topology, the total topology is derived on this basis. The above six structures are the most basic topological model, which is a topology model with a single power generation device and a chargeable and discharge device.

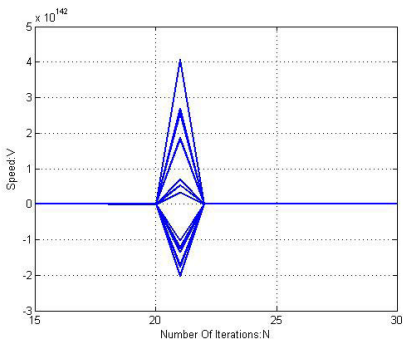For devices in an n-type topology, this paper is divided into two categories, one for devices that are only used for output, assuming that the number is m, one class refers to devices that are available for output and input, assuming that the number is n, the total topology map generated is 2m*3n. These general topologies are based on the above. The basic topology is constantly evolving, Figure34 studies above topologies. The general topology changes are linear for the basic structure. The general rule can also be drawn.

## V. CONCLUSION

This paper defines the equivalence of the complex smart grid system model for the first time, and provides the model with N nodes smart grid. Firstly, a new method for brittleness analysis of complex smart grids is proposed. Secondly, the weighted graph model of the brittle relationship of complex smart grid systems is analyzed. Finally, the model characteristics of logical clarity, hierarchical representation, qualitative analysis are proposed. The most likely collapse path is analyzed through the maximum voltage collapse path under different equivalent modes. Results and conclusions drawn from this study are also presented. The research of voltage collapse path analysis will be more meaningful for multi energy access, especially for smart grid with high proportion of energy access.

## REFERENCES

[1] R. E. C. Gutiérrez and J. M. Ramirez, "Voltage collapse detection based on local measurements," *Electr. Power Syst. Res.*, vol. 107, pp. 77–84, Feb. 2014.
[2] Q. Li, H. Zhang, and D. Ling, "The model and analyzing method for complex system's brittleness," *Syst. Eng.*, vol. 23, no. 1, pp. 9–12, 2005.

[3] Y. Wang, I. R. Pordanjani, W. Li, W. Xu, T. Chen, E. Vaahedi, and J. Gurney, "Voltage stability monitoring based on the concept of coupled single-port circuit," *IEEE Trans. Power Syst.*, vol. 26, no. 4, pp. 2157–2163, Nov. 2011.

[4] J. W. Simpson-Porco and F. Bullo, "Distributed monitoring of voltage collapse sensitivity indices," *IEEE Trans. Smart Grid*, vol. 7, no. 4, pp. 1979–1988, Jul. 2016.

[5] R. Cheng and Z. Zhu, "Research on brittleness of complex ship power electric system based on particle swarm optimization," *Modern Electr. Technique*, vol. 35, no. 1, pp. 135–138, 2012.

[6] H. Z. Jin, L. M. Yan, P. X. Rong, X. B. Lin, and M. Li, "Brittleness analysis of electric network," in *Proc. 4th Int. Conf. Eng. Appl. Comput. Algorithms*. Guelph, ON, Canada: Watam Press, 2005, pp. 32–36.

[7] D.-M. Lin, H.-Z. Jin, Q. Li, and H.-M. Wu, "The brittleness model of complex system based on cellular automata," *J. Mar. Sci. Appl.*, vol. 3, no. 2, pp. 69–72, Dec. 2004.

[8] M. Karimi, A. Shahriari, M. R. Aghamohammadi, H. Marzooghi, and V. Terzija, "Application of Newton-based load flow methods for determining steady-state condition of well and ill-conditioned power systems: A review," *Int. J. Electr. Power Energy Syst.*, vol. 113, pp. 298–309, Dec. 2019.

[9] M. R. C. Acosta, S. Ahmed, C. E. Garcia, and I. Koo, "Extremely randomized trees-based scheme for stealthy cyber-attack detection in smart grid networks," *IEEE Access*, vol. 8, pp. 19921–19933, 2020.

[10] S. D. Beigvand, H. Abdi, and S. N. Singh, "Voltage stability analysis in radial smart distribution grids," *IET Gener., Transmiss. Distrib.*, vol. 11, no. 15, pp. 3722–3730, Oct. 2017.

[11] Y. Xu, R. Zhang, J. Zhao, Z. Y. Dong, D. Wang, H. Yang, and K. P. Wong, "Assessing short-term voltage stability of electric power systems by a hierarchical intelligent system," *IEEE Trans. Neural Netw. Learn. Syst.*, vol. 27, no. 8, pp. 1686–1696, Sep. 2016.

[12] L. Lee and P. Hu, "Vulnerability analysis of cascading dynamics in smart grids under load redistribution attacks," *Int. J. Electr. Power Energy Syst.*, vol. 111, pp. 182–190, Oct. 2019.

[13] S.-S. Seo, S.-G. Kang, B.-J. Lee, T.-K. Kim, and H.-C. Song, "Determination of reactive power compensation considering large disturbances for power flow solvability in the Korean power system," *J. Electr. Eng. Technol.*, vol. 6, no. 2, pp. 147–153, Mar. 2011.

[14] M. H. Fan, C. S. Wang, and V. Ajjarapu, "Power system equilibrium tracing and bifurcation detection based on the continuation of the recursive projection method," *IET Gener., Transmiss. Distribution*, vol. 6, no. 3, p. 199, 2012.

[15] R. Tiwari, K. R. Niazi, and V. Gupta, "Line collapse proximity index for prediction of voltage collapse in power systems," *Int. J. Electr. Power Energy Syst.*, vol. 41, no. 1, pp. 105–111, Oct. 2012.

[16] M. Derafshian, N. Amjady, and S. Dehghan, "Special protection scheme against voltage collapse," *IET Gener., Transmiss. Distrib.*, vol. 10, no. 2, pp. 341–351, 2016.

[17] C. Church, W. G. Morsi, M. E. El-Hawary, C. P. Diduch, and L. C. Chang, "Voltage collapse detection using ant colony optimization for smart grid applications," *Electr. Power Syst. Res.*, vol. 81, no. 8, pp. 1723–1730, Aug. 2011.

[18] R. Preece, N. C. Woolley, and J. V. Milanović, "The probabilistic collocation method for power-system damping and voltage collapse studies in the presence of uncertainties," *IEEE Trans. Power Syst.*, vol. 28, no. 3, pp. 2253–2262, Aug. 2013.

[19] S. Wang, Q. Mao, J. Xu, Y. Ge, and S. Liu, "An improved mathematical model of photovoltaic cells based on datasheet information," *Sol. Energy*, vol. 199, pp. 437–466, Mar. 2020.

[20] G. Catalina, G. Antonio, and D. Antonio, "Individual branch and path necessary conditions for saddle-node bifurcation voltage collapse," *IEEE Tran. Smart Grid*, vol. 3, no. 2, pp. 986–995, Aug. 2012.

[21] S. Grijalva, "Individual branch and path necessary conditions for saddle-node bifurcation voltage collapse," *IEEE Trans. Power Syst.*, vol. 27, no. 1, pp. 12–19, Feb. 2012.

[22] A. Mahari and H. Seyedi, "A wide area synchrophasor-based load shedding scheme to prevent voltage collapse," *Int. J. Electr. Power Energy Syst.*, vol. 78, pp. 248–257, Jun. 2016.

[23] X. Li, L. Zhang, T. Jiang, F. Li, H. Chen, and H. Jia, "Relaxed decoupled direct calculation of voltage collapse points and its application in static voltage stability region boundary formation," *Electr. Power Energy Syst.*, vol. 125, Feb. 2021, Art. no. 106452.

[24] T. Burle and V. V. S. B. R. Chintapalli, "Effect of ambient temperature variations on estimation of proximity of the voltage collapse point," *IET Gener., Transmiss. Distrib.*, vol. 14, no. 25, pp. 6382–6396, Dec. 2020.

[25] R. Małkowski, M. Izdebski, and P. Miller, "Adaptive algorithm of a tap-changer controller of the power transformer supplying the radial network reducing the risk of voltage collapse robert," *Energies*, vol. 13, no. 20, pp. 1–25. 2020.

[26] V. Gundu, S. P. Simon, K. Sundareswaran, and S. R. N. Panugothu, "Gated recurrent unit based demand response for preventing voltage collapse in a distribution system," *Turkish J. Elect. Eng. Comput. Sci.*, vol. 28, no. 6, pp. 3319–3334, 2020.

[27] E. Ghahremani, A. Heniche-Oussedik, M. Perron, M. Racine, S. Landry, and H. Akremi, "A detailed presentation of an innovative local and wide-area special protection scheme to avoid voltage collapse: From proof of concept to grid implementation," *IEEE Trans. Smart Grid*, vol. 10, no. 5, pp. 5196–5211, Sep. 2019.

[28] A. Javadi, L. Woodward, and K. Al-Haddad, "Real-time implementation of a three-phase THSeAF based on a VSC and a P+R controller to improve the power quality of weak distribution systems," *IEEE Trans. Power Electron.*, vol. 33, no. 3, pp. 2073–2082, Mar. 2018.

[29] S. Elphick, P. Ciufo, G. Drury, V. Smith, S. Perera, and V. Gosbell, "Large scale proactive power-quality monitoring: An example from Australia," *IEEE Trans. Power Del.*, vol. 32, no. 2, pp. 881–889, Apr. 2017.

[30] J. M. Guerrero, "Special issue on power quality in smart grids," *IEEE Trans. Smart grid*, vol. 8, no. 1, pp. 379–381, Dec. 2017.

[31] C. X. Dou, T. Gui, Y. F. Bi, J. Z. Yang, and X. G. Li, "Assessment of power quality based on DS evidence theory," *Int. J. Automat. Comput.*, vol. 11, no. 6, pp. 635–643, 2014.

[32] X. L. Wang, X. Qin, D. X. Liu, Z. J. Wang, J. Wang, H. M. Xu, and M. Qin, "Power system data quality evaluation based on the analytic hierarchy process," *Adv. Mater. Res.*, vols. 712–715, pp. 2611–2614, Jun. 2013.

[33] J. Yin, X. Liang, C. Xiao, R. Wei, and S. Chen, "The application of matter-element extension method based on gray clustering theory in the groundwater quality assessment of Jilin City," in *Proc. Int. Symp. Env.*, vol. 3, 2011, pp. 2100–2103.

[34] S. Zhang, Y. Hu, and C. Wang, "Evaluation of borrower's credit of P2P loan based on adaptive particle swarm optimisation BP neural network," *Int. J. Comput. Sci. Eng.*, vol. 19, no. 2, pp. 197–205, 2019.

[35] X. Gu, Q. Shen, and P. P. Angelov, "Particle swarm optimized autonomous learning fuzzy system," *IEEE Trans. Cybern.*, early access, Feb. 20, 2020, doi: 10.1109/TCYB.2020.2967462.

[36] M. C. Pulcherio, A. A. Renjit, M. S. Illindala, A. S. Khalsa, J. H. Eto, D. A. Klapp, and R. H. Lasseter, "Evaluation of control methods to prevent collapse of a mixed-source microgrid," *IEEE Trans. Ind. Appl.*, vol. 52, no. 6, pp. 4566–4576, Nov. 2016.

**JIE XU** (Member, IEEE) received the M.D. degree from the Anhui University of Technology, in 2008, and the Ph.D. degree from the University of Science and Technology of China, in 2017. He is currently a Lecturer with the Department of Electronic Engineering, Anhui Polytechnic University. His research interests include electric engineering and automation, smart grid, and power quality application in the future grid.

**WENGEN GAO** is currently pursuing the Ph.D. degree with Jiangnan University. He is currently an Associate Professor with the Department of Electronic Engineering, Anhui Polytechnic University, Wuhu, China. His research interests include smart grid and power electronics technology.

• • •